High-pressure synthesis and luminescent properties of cubic ZnO/MgO nanocomposites

A. N. Baranov,[1] O. O. Kurakevych,[2] V. A. Tafeenko,[1] P. S. Sokolov,[2,3] G. N. Panin,[4,5] and V. L. Solozhenko[2,a)]
[1]*Department of Chemistry, Moscow State University, 119992 Moscow, Russia*
[2]*LPMTM-CNRS, Université Paris Nord, 93430 Villetaneuse, France*
[3]*Department of Materials Science, Moscow State University, 119992 Moscow, Russia*
[4]*Department of Physics, Quantum-Functional Semiconductor Research Center, Dongguk University, Seoul 100-715, Republic of Korea*
[5]*Institute of Microelectronics Technology and High Purity Materials, RAS, Chernogolovka, Moscow distr. 142432 Russia*

(Received 20 January 2010; accepted 10 February 2010; published online 12 April 2010)

The formation of the nanocrystalline rocksalt ZnO (rs-ZnO) has been *in situ* studied by x-ray diffraction with synchrotron radiation at high pressure and high temperature. A number of rs-ZnO/MgO nanocomposites with preset grain size were synthesized at 7 GPa and 800 K starting from wurtzite ZnO nanoparticles or nanorods. The use of MgO matrix allowed us to recover metastable rs-ZnO in the nanocrystalline form at ambient pressure. The cathodoluminescence measurements demonstrated the blue shift in the luminescence of rs-ZnO nanocrystals down to 402–408 nm that can be attributed to the enhanced incorporation of point defects with lower activation energy. © *2010 American Institute of Physics*. [doi:10.1063/1.3359661]

I. INTRODUCTION

ZnO is a promising luminescent semiconductor with a wide direct band gap (3.37 eV for wurtzite structure) and a high exciton binding energy (60 meV),[1,2] while ZnO-based nanostructured materials are attractive for the fabrication of optoelectronic devices operating in the blue and ultraviolet spectral regions. At ambient conditions, the thermodynamically stable phase of ZnO has a hexagonal wurtzite structure with fourfold tetrahedral coordination (w-ZnO phase). The high-pressure cubic rocksalt structure with sixfold coordination (rs-ZnO phase) seems promising for electronic and spintronics applications because of its ability to incorporate much higher amount of doping atoms and native point defects than the wurtzite ZnO.

Similarly to many other II-VI compounds with wurtzite structure, w-ZnO undergoes phase transition under high pressures into the denser rs-ZnO.[3] At room temperature, the phase transition of bulk w-ZnO occurs at about 9 GPa.[4] The transition pressure depends on both temperature[5] and crystal size.[6] Upon decompression, the reverse transition of rs-ZnO into w-ZnO takes place at about 2 GPa at room temperature, that render impossible to recover the pure high-pressure rs-ZnO at ambient conditions. However, it has been reported that the nanocrystalline rs-ZnO can be quenched from 15 GPa and 550 K down to ambient conditions in a diamond anvil cell.[7] At present time it is not clear whether this stabilization should be attributed to the grain nanosize or to the residual strains in the quenched sample. The existence of rs-ZnO nanocrystals at ambient pressure has been proved by the transmission electron microscopy (TEM) study of MgO single crystals coimplanted by zinc and oxygen ions.[8] The properties of rs-ZnO are still not studied. Even rs-ZnO band gap, the value of outmost importance for optical and electronic applications, has not been experimentally determined. From theoretical calculations, the rs-ZnO indirect band gap can vary from 2.36 to 4.51 eV.[9–11] The only high-pressure study of the optical properties of rs-ZnO (Ref. 12) indicated that this phase is an indirect gap semiconductor with a band gap of 2.45 eV at 13.5 GPa.

Recently it has been shown that stable $Mg_xZn_{1-x}O$ solid solutions ($0.32 \leq x \leq 0.67$) with rocksalt structure can be synthesized at pressures above 7 GPa and temperatures above 1600 K.[13]

Lattice parameter of the magnesium oxide (a_{MgO} =4.2112 Å, space group *Fm*3*m* according to JCPDS No. 45–0946) is slightly less than that of the rocksalt zinc oxide, ($a_{rs\text{-}ZnO}$=4.280 Å, space group *Fm*3*m* according to Ref. 14), so that the MgO can be used as a matrix (supporting material) for metastable rocksalt ZnO nanoparticle (NP).

Here we report the first successful high pressure-high temperature synthesis of rs-ZnO nanocrystals with controlled grain size that are stable at ambient conditions in the form of rs-ZnO/MgO nanocomposites.

II. EXPERIMENTAL DETAILS

A. Synthesis of wurtzite ZnO/MgO nanocomposites

The precursors, i.e., w-ZnO/MgO nanocomposites, have been synthesized by several methods in order to prepare nanocrystals of different size and/or with different form factor. The size and morphology of the nanocrystals are given in the Table I.

Sample NP10. Zinc and magnesium acetates (1:4 molar ratio) were dissolved in methanol and mixed with sodium hydroxide solution in methanol. After centrifuging and washing (5 times) the obtained precipitate was annealed at 670 K

a)Electronic mail: vls@lpmtm.univ-paris13.fr.

TABLE I. Results of scanning electron microscopy (SEM) and TEM analysis of pristine wurtzite ZnO/MgO composites.

Precursor	Average size of w-ZnO NP and diameter/length of NR (nm)
NP10	10 ± 3 (TEM data)
NP50	53 ± 9 (SEM data)
NP200	169 ± 8 (SEM data)
NR	50/(500–1000) (SEM data)

for 3 h. This method allowed to produce the ZnO NP of less than 10 nm in size distributed in magnesium oxide matrix as shown in Fig. 1(a). It should be noted that MgO is considered as a barrier layer preventing the agglomeration of individual ZnO particles during the thermal processing. As can be seen in Fig. 1(a) (inset), the selected area electron diffraction pattern shows reflections of both w-ZnO and MgO phases. The size of the zones of coherent scattering according to the Scherrer equation is equal to 10(2) nm that well agrees with the TEM observations.

Sample NP50. The ZnO nanopowder with an average particle size of about 50 nm was prepared by the following procedure. Zinc carbonate hydroxide (ZCH) was obtained by precipitation from an aqueous solution of zinc nitrate by excess of ammonium carbonate. The precipitate was centrifuged, thoroughly washed in distilled water and freeze dried. A mixture of the ZCH with NaCl was milled for 1 h and annealed in a muffle furnace at 970 K. NaCl was washed out with distilled water. The as-prepared ZnO nanopowder was then dispersed in the methanol solution of magnesium acetate in the ZnO/MgO molar ratio1:4 using ultrasonic bath, and mixed with the equivalent amount of sodium hydroxide solution in methanol. After centrifuging and washing (5 times) the residue was decomposed at 670 K for 6 h in order to obtain 50 nm NP of ZnO in MgO matrix.

Sample NP200. Monodispersed ZnO spherical particles of 170 nm in size [Fig. 1(c)] were prepared by hydrolysis of zinc acetate dihydrate ($ZnAc_2$ $2H_2O$) by a two-stage process.[15] 0.01 mol of $ZnAc_2$ $2H_2O$ was dissolved in 100 ml of diethylene glycol. The clear solution was heated up to 430 K, then stirred for one hour and cooled down to room temperature. Resulting precipitate was washed thoroughly with distilled water and dried. The as-prepared powder was dispersed in the methanol solution of magnesium acetate in the ZnO/MgO molar ratio1:4, and then reprecipitated by equivalent amount of sodium hydroxide solution in methanol. The residue was subsequently decomposed as described above.

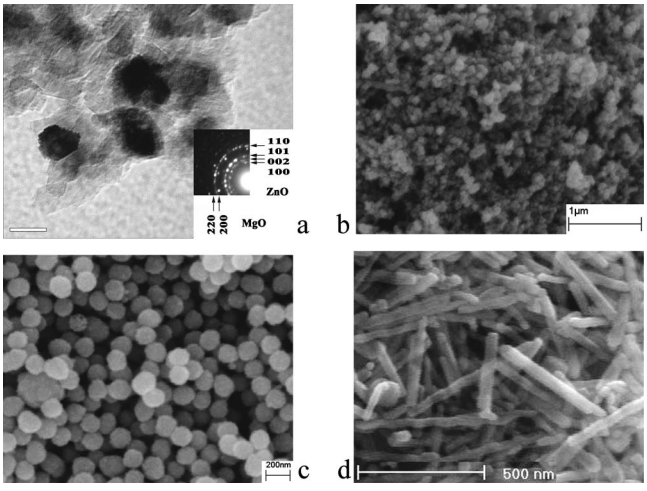

FIG. 1. SEM pictures of the precursors: (a) w-ZnO/MgO nanocomposite (NP10 sample); (b) uniform (~53 nm) w-ZnO NP (NP50 sample); (c) uniform (~170 nm) w-ZnO particles (NP200 sample), and (d) w-ZnO NR (NR sample). Inset: SAED pattern of NP10 sample.

Sample NR. w-ZnO nanorods (NR) (each nanorod is a single-crystal NP) were synthesized by the method described in Ref. 16. w-ZnO NR—MgO composite was prepared as described above for NP200.

B. High-pressure experiments

In situ experiments up to 5 GPa have been performed using MAX80 multianvil x-ray system at beamline F2.1, DORIS III (HASYLAB-DESY). The experimental details and high-pressure setup have been described elsewhere.[17] Energy-dispersive x-ray diffraction (XRD) patterns were collected on a Canberra solid state Ge-detector with fixed Bragg angle $2\theta = 9.26(1)^\circ$ using a white beam collimated down to 100×100 μm^2. The sample temperature was measured by a Pt10%Rh-Pt thermocouple without correction for the pressure effect on the thermocouple emf. The samples were compressed to the required pressure at ambient temperature, and then diffraction patterns were collected upon stepwise heating (25-or 50-K steps). With the storage ring operating at 4.44 GeV and 120 ± 30 mA, the time of data collection for each pattern was about 3 min.

Quenching experiments at 7 GPa have been performed using a cubic multianvil press at LPMTM-CNRS. Gold capsules were used to prevent contamination of the samples.

C. XRD study

Quenched samples were studied by the powder XRD using STOE diffractometer, Cu $K\alpha$ radiation, PSD-detector, $2\Theta < 130^\circ$. The FULLPROF SUITE and WINPLOTR software[18,19] have been used for data processing. Powder diffraction profiles were fitted using the pseudo-Voight (p-V) profile function in TCH modification.[20] Each reflection profile was characterized by its full width at half maximum (FWHM) and η, a mixing parameter of Gaussian and Lorenzian components of the pV profile function expressed as $pV = \eta L + (1 - \eta G)]$. The H_G and H_L values are FWHM of Gaussian and Lorentzian profiles of the Voight function, respectively. The microstructure (size and strain) within FULLPROF program was treated using instrumental function with H_{G_inst} and H_{L_inst} parameters calculated from the diffraction pattern of LaB_6 standard.

D. Characterization of the recovered samples

The microstructure of the samples was characterized by TEM in the bright-field mode using JEOL (JEM-2010) transmission electron microscope operating at 200 kV. Powdered samples were dispersed in droplets of ethanol and then loaded on copper grids coated with a carbon film. Cathodoluminescence (CL) spectra were collected at room tempera-

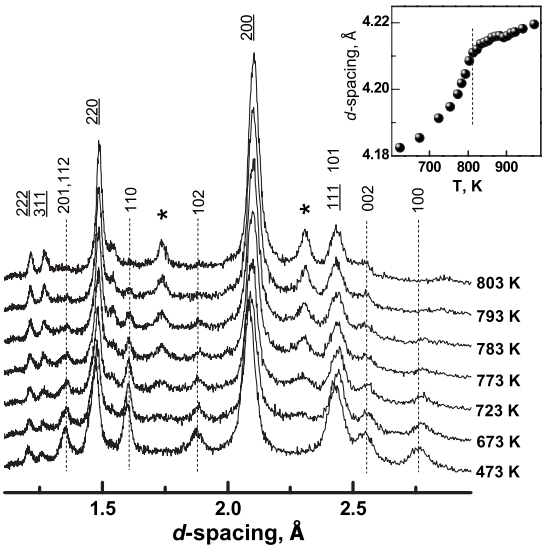

FIG. 2. Diffraction patterns of the NP10 sample taken at 4.8 GPa at different temperatures. Underlined indexes correspond to MgO and rs-ZnO reflections, while nonunderlined indexes to w-ZnO. Asterisks denote the lines of $Mg(OH)_2$ impurity. (Inset: position of *200* line (MgO+rs-ZnO) vs temperature).

ture using XL 30S FEG high-resolution scanning electron microscope with a mono-CL system in the 300–900 nm wavelength range.

III. RESULTS AND DISCUSSION

The ZnO-MgO system has been *in situ* studied at pressures about 5 GPa using XRD with synchrotron radiation in order to determine the optimal temperature range for the synthesis of rs-ZnO/MgO nanocomposites without formation of the corresponding solid solutions.[21] The diffraction patterns of the NP10 sample taken at 4.8 GPa in the course of temperature increase are shown in Fig. 2.

One can see that intensities of *100*, *002*, and *102* lines of w-ZnO significantly decrease with temperature increase, and *200* and *220* lines of both rs-ZnO and MgO phases shift to higher d-spacings. The position of the most intensive *200* line versus temperature is plotted in inset. Since lattice parameters of rs-ZnO and MgO phases are very close, the lines of these two phases cannot be resolved in energy-dispersive XRD patterns taken *in situ* at high pressures. However, the singular point on the dependence of *200* line position versus temperature should reflect the structural/compositional alterations in rs-ZnO phase upon heating, while at the same conditions MgO undergoes quasilinear thermal expansion only. The temperature dependence of the *200* line position consists of two parts; exponential and linear ones. An exponential increase in the plotted values of peak position at low temperatures indicates the formation of the rs-ZnO phase (increasing amount of cubic phase). The singular point separating the exponential and linear parts of the curve corresponds to the complete disappearance of w-ZnO at given pressure and may be determined as the completion temperature of the w-ZnO to rs-ZnO phase transition i.e., $T_c = 800$ K. The linear part of the curve at higher temperatures reflects thermal expansion of both MgO and rs-ZnO phases.

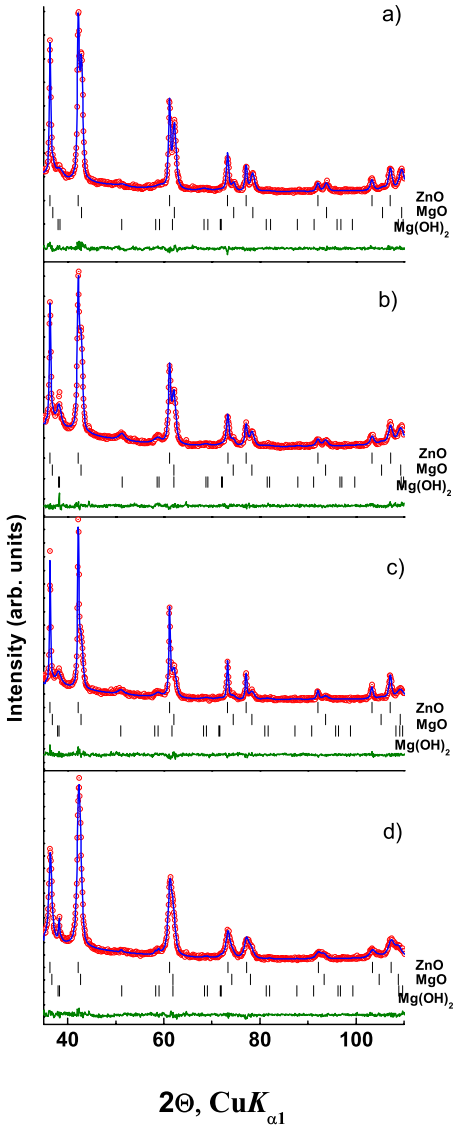

FIG. 3. (Color online) The observed and calculated XRD patterns of recovered rs-ZnO/MgO nanocomposites after the refinement procedure (Rietveld method for rs-ZnO and MgO phases and Le Bail method for $Mg(OH)_2$) [(a)—NR, (b)—NP200, (c)—NP50, and (d)—NP10]. The set of vertical bars indicates the calculated position of Braggs peaks for ZnO, MgO and $Mg(OH)_2$. The discrepancies between observed and calculated profiles are very small and all residuals indicate that the unit cell parameters are accurately determined (Rp for the whole profile is within 3.5%–4.5%).

Figure 3 shows the angle-dispersive diffraction patterns of the samples recovered from 800 K and 7 GPa. The lines of w-ZnO phase disappeared completely and the line positions in the diffraction patterns correspond to rs-ZnO and MgO. Some patterns exhibit additional weak lines with relative intensities less then 2% because of possible surface reaction of MgO with moisture during the sample preparation. The lines of impurities have been indexed in the framework of hexagonal unit cell with lattice parameters $a = 3.15$ Å and $c = 4.69$ Å using DICVOL software.[22] These parameters coincided with those of $Mg(OH)_2$. No lines of other phases have been detected.

For the structure refinement we have used approach based on the extraction of integrated intensities from diffraction pattern after Rietveld or Le Bail fitting with subsequent

TABLE II. Results of the Rietveld refinement of atomic parameters for the phases in the rs-ZnO/MgO composites.

	a (ZnO) (Å)	*a* (MgO) (Å)	$U_{iso\text{-}metal}$ (ZnO/MgO) ($Å^2$)	$U_{iso\text{-}oxygen}$ (ZnO/MgO) ($Å^2$)	Occupancy (metal) in ZnO/MgO*	R (ZnO/MgO) (%)
NP10	4.2756(2)	4.2351(2)	0.018(1)/0.030(1)	0.014(3)/0.032(1)	0.96(6)/1.0	1.0/1.0
NP50	4.28222(5)	4.22569(9)	0.017(1)/0.020(1)	0.014(3)/0.020(4)	1.0(3)/1.0	1.2/1.5
NP200	4.28012(8)	4.22391(9)	0.018(2)/0.025(2)	0.017(3)/0.023(4)	0.98(8)/1.0	0.3/1.0
NR	4.28084(9)	4.21791(8)	0.019(2)/0.023(3)	0.018(2)/0.021(3)	0.98(4)/1.0	0.9/0.9

refinement of atomic parameters using SHELX97 software.[23] Earlier this approach has been successfully used for refinement of atomic parameter of $Zn_xMg_{1-x}O$ solid solutions.[24] The unit cell parameters of ZnO/MgO nanocomposites, atom displacements (U_{iso}) as well as atom occupancy parameters and final R-factors are given in Table II. The use of the integrated intensities for the refinement of the atom parameters gave much better, self-consistent and reasonable results in comparison with Rietveld method. The values of the cell parameters well agree with those of the pure Zn and Mg oxides except NP10 sample, for which we suggest the formation of cubic $Zn_xMg_{1-x}O$ solid solution with a very small x value.

According to TEM data, the recovered NP10 samples consist of the individual ZnO and MgO particles [Fig. 4(a); ZnO is darker than MgO]. The particle size varies from 7 to 13 nm for ZnO and from 20 to 40 nm for MgO, thus no change in ZnO grain size was observed in the course of w-ZnO to rs-ZnO phase transformation [selected area electron diffraction (SAED) pattern in Fig. 4(d) shows complete disappearance of w-ZnO reflections in the recovered sample]. The lattice fringes of the cores are adjusted with those of MgO matrix reflecting the effect of rs-ZnO phase stabilization [Fig. 4(a)]. The element distribution maps recorded using the Scanning Transmission Electron Microscopy-Energy-Dispersive Spectrometry (STEM-EDS) method are shown in Figs. 4(b) and 4(c) indicating the presence of separate ZnO and MgO particles. The SAED pattern of recovered NR sample [Fig. 4(e)] shows the single-crystal nature of quenched rs-ZnO NR contrary to the polycrystalline MgO matrix.

Figure 5 shows CL spectra of recovered rs-ZnO-based nanocomposites as well as CL spectra of the precursors. All starting w-ZnO/MgO precursors show blue luminescence in the range of 410–446 nm. The peaks at 446 (NP10), 410 (NP50), 420 (NP200), and 414 nm (NR) could be attributed to a donor-acceptor pair transitions.[25] The pressure-induced phase transition in w-ZnO/MgO nanocomposites leads to the remarkable changes in the luminescent properties, i.e., all recovered rs-ZnO/MgO samples show the blue shifted luminescence of lower intensity in comparison to the w-ZnO

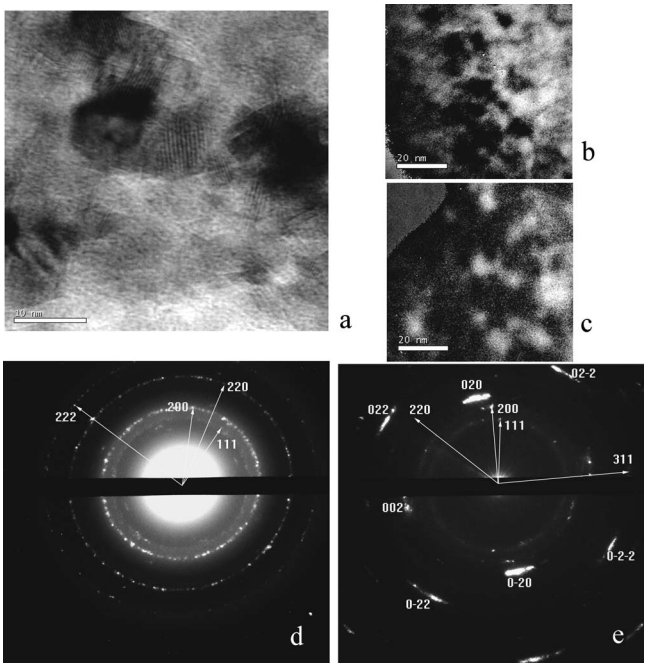

FIG. 4. TEM bright field image of the recovered NP10 sample (a), elemental distribution maps [(b) and (c) for magnesium and zinc, respectively,] and SAED patterns taken from NP10 (d) and NR (e) samples.

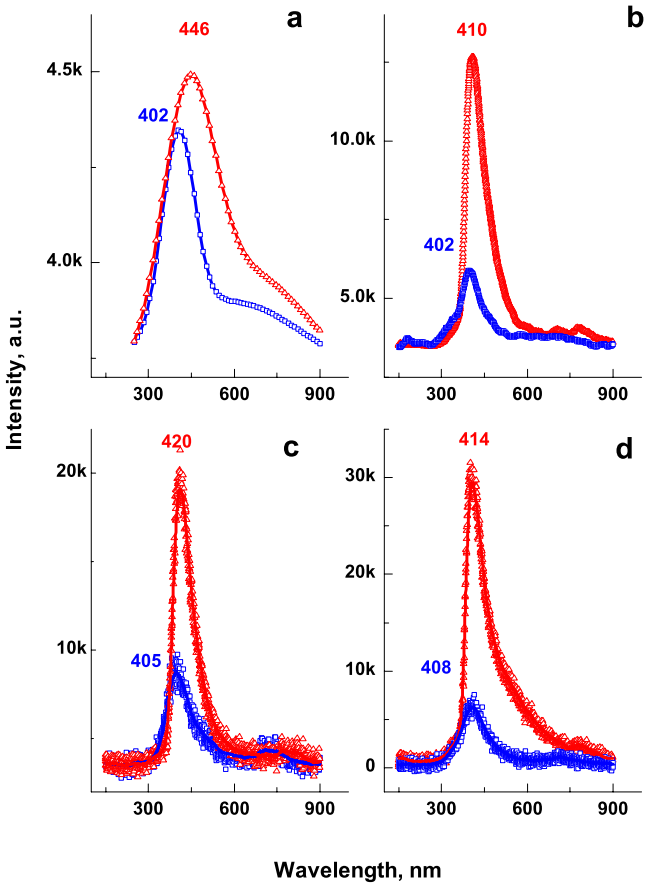

FIG. 5. (Color online) CL spectra of rs-ZnO/MgO composites synthesized at 7 GPa and 800 K (blue circles) in comparison with starting materials (red triangles): (a) NP10, (b) NP50, (c) NP200, and (d) NR.

based nanocomposites. The change in luminescence from ZnO/MgO samples is evidently the result of phase transformation leading to enhanced incorporation of impurities or/and native point defects into the ZnO crystal lattice. The rs-ZnO phase is expected to be more easily affected to impurity incorporation as compared with w-ZnO. The higher density of acceptors/donors and their lower activation energies have been expected for the cubic structure. The observed blue shift in the defect-related peaks in CL spectra of rs-ZnO nanocomposites could indicate the higher incorporation of defects such as V_{Zn}-related complexes in the synthesized cubic nanocrystals and hence a probability of the higher p-type doping. The blue luminescence from ZnO NP has been usually attributed to transitions between Zn interstitial (Zn_i) and Zn vacancy (V_{Zn}) levels.[26] In our case rs-ZnO/MgO nanocomposites show the blue-shifted luminescence with lower intensity indicating the higher defect incorporation density and the higher concentration of free carriers.

IV. CONCLUSIONS

As a result of the present study, we have shown that rs-ZnO/MgO nanocomposites with different ZnO particle size can be synthesized at high pressures and temperatures and quenched down to ambient conditions. According to the Rietveld analysis of XRD data, the lattice parameters of ZnO and MgO phases in the nanocomposites are in good agreement with corresponding values of the bulk substances. CL spectra of the recovered samples at room temperature show the blue shift in the luminescence peaks due to the formation of rs-ZnO phase with higher incorporation of point defects (V_{Zn}-related complexes) with lower activation energy compared to w-ZnO which can be used for fabrication of p-type rs-ZnO materials with high hole concentration.

ACKNOWLEDGMENTS

The authors thank Dr. C. Lathe for the assistance in high-pressure experiments and V. Richard for TEM studies. Experiments at HASYLAB-DESY have been performed during beamtime allocated to the Project No. I-20070033 EC and have received funding from the European Community's Seventh Framework Programme (FP7/2007-2013) under Grant No. 226716. This work was also supported by the Russian Foundation for Basic Research (Project No. 09-03-90442-Укр_ф_а). PSS is grateful to the French Ministry of Foreign Affairs for financial support (BGF fellowship No 2007 1572).

[1] S. J. Pearton, D. P. Norton, K. Ip, Y. W. Heo, and T. Steiner, Prog. Mater. Sci. **50**, 293 (2005).
[2] Ü. Özgür, Ya. I. Alivov, C. Liu, A. Teke, M. A. Reshchikov, S. Dogan, V. Avrutin, S. J. Cho, and H. Morkoc, J. Appl. Phys. **98**, 041301 (2005).
[3] A. Mujica, A. Rubio, A. Munoz, and R. J. Needs, Rev. Mod. Phys. **75**, 863 (2003).
[4] C. H. Bates, W. B. White and R. Roy, Science **137**, 993 (1962).
[5] K. Kusaba, Y. Syono, and T. Kikegawa, Proc. Jpn. Acad., Ser. B: Phys. Biol. Sci. **75**, 1 (1999).
[6] J. Z. Jiang, J. S. Olsen, L. Gerward, D. Frost, D. Rubie, and J. Peyronneau, Europhys. Lett. **50**, 48 (2000).
[7] F. Decremps, J. Pellicer-Porres, F. Datchi, J. P. Itie, A. Polian, F. Baudelet, and J. Jiang, Appl. Phys. Lett. **81**, 4820 (2002).
[8] S. W. H. Eijt, J. de Roode, H. Schut, B. J. Kooi, and J. Th. M. De Hosson, Appl. Phys. Lett. **91**, 201906 (2007).
[9] J. E. Jaffe, R. Pandey, and A. B. Kunz, Phys. Rev. B **43**, 14030 (1991).
[10] J. Cai, and N. Chen, J. Phys. Condens. Matter **19**, 266207 (2007).
[11] H. Q. Ni, Y. F. Lu, and Z. M. Ren, J. Appl. Phys. **91**, 1339 (2002).
[12] A. Segura, J. A. Sans, F. J. Manjon, A. Munoz, and M. J. Herrera-Cabrera, Appl. Phys. Lett. **83**, 278 (2003).
[13] A. N. Baranov, V. L. Solozhenko, C. Chateau, G. Bocquillon, J. P. Petitet, G. N. Panin, T. W. Kang, R. V. Shpanchenko, E. V. Antipov, and Y. J. Oh, J. Phys. Condens. Matter **17**, 3377 (2005).
[14] S. Desgreniers, Phys. Rev. B **58**, 14102 (1998).
[15] E. W. Seelig, B. Tang, and R. P. H. Chang, A. Yamilov, and H. Cao, Mater. Chem. Phys. **80**, 257 (2003).
[16] A. N. Baranov, G. N. Panin, T. W. Kang, and Y. J. Oh, Nanotechnology **16**, 1918 (2005).
[17] V. L. Solozhenko, A. N. Baranov, and V. Z. Turkevich, Solid State Commun. **138**, 534 (2006).
[18] J. Rodriguez-Carvajal, Physica B **192**, 55 (1993).
[19] J. Roiznel and T. Rodriguez-Carvajal, Proceedings of the European Powder Diffraction Conference (EPDIC7), 2001, Vol. 378, p. 118.
[20] P. Thompson, D. E. Cox, and J. B. Hastings, J. Appl. Crystallogr. **20**, 79 (1987).
[21] G. N. Panin, A. N. Baranov, Y. J. Oh, T. W. Kang, and T. W. Kim, J. Cryst. Growth **279**, 494 (2005).
[22] A. Boultif and D. Louer, J. Appl. Crystallogr. **24**, 987 (1991).
[23] G. M. Sheldrick, *SHELX* (University of Gottingen, Germany, 1997).
[24] S. I. Gurskiy, V. A. Tafeenko, and A. N. Baranov, Russ. J. Inorg. Chem. **53**, 111 (2008).
[25] M. K. Ryu, S. H. Lee, M. S. Jang, G. N. Panin, and T. W. Kang, J. Appl. Phys. **92**, 154 (2002).
[26] Q. Ou, T. Matsuda, M. Mesko, A. Ogino, and M. Nagatsu, Jpn. J. Appl. Phys. **47**, 389 (2008).